NeuroImage: Clinical 20 (2018) 772–782

Contents lists available at ScienceDirect

NeuroImage: Clinical

journal homepage: www.elsevier.com/locate/ynicl

Abnormal neurite density and orientation dispersion in unilateral temporal lobe epilepsy detected by advanced diffusion imaging

Daichi Sone[a,*], Noriko Sato[b], Miho Ota[c], Norihide Maikusa[a], Yukio Kimura[b], Hiroshi Matsuda[a]

[a] Integrate Brain Imaging Center, National Center of Neurology and Psychiatry, Tokyo, Japan
[b] Department of Radiology, National Center of Neurology and Psychiatry, Tokyo, Japan
[c] Department of Neuropsychiatry, Division of Clinical Medicine, Faculty of Medicine, University of Tsukuba, Ibaraki, Japan

ARTICLE INFO

Keywords:
Temporal lobe epilepsy
Neurite orientation dispersion and density imaging
Diffusion MRI
MRI-negative focal epilepsy
Hippocampal sclerosis

ABSTRACT

Background: Despite recent advances in diffusion MRI (dMRI), there is still limited information on neurite orientation dispersion and density imaging (NODDI) in temporal lobe epilepsy (TLE). This study aimed to demonstrate neurite density and dispersion in TLE with and without hippocampal sclerosis (HS) using whole-brain voxel-wise analyses.

Material and methods: We recruited 33 patients with unilateral TLE (16 left, 17 right), including 14 patients with HS (TLE-HS) and 19 MRI-negative ^{18}F-fluorodeoxyglucose positron emission tomography (FDG-PET)-positive patients (MRI-/PET+ TLE). The NODDI toolbox calculated the intracellular volume fraction (ICVF) and orientation dispersion index (ODI). Conventional dMRI metrics, that is, fractional anisotropy (FA) and mean diffusivity (MD), were also estimated. After spatial normalization, all dMRI parameters (ICVF, ODI, FA, and MD) of the patients were compared with those of age- and sex-matched healthy controls using Statistical Parametric Mapping 12 (SPM12). As a complementary analysis, we added an atlas-based region of interest (ROI) analysis of relevant white matter tracts using tract-based spatial statistics.

Results: We found decreased neurite density mainly in the ipsilateral temporal areas of both right and left TLE, with the right TLE showing more severe and widespread abnormalities. In addition, etiology-specific analyses revealed a localized reduction in ICVF (i.e., neurite density) in the ipsilateral temporal pole in MRI-/PET+ TLE, whereas TLE-HS presented greater abnormalities, including FA and MD, in addition to a localized hippocampal reduction in ODI. The results of the atlas-based ROI analysis were consistent with the results of the SPM12 analysis.

Conclusion: NODDI may provide clinically relevant information as well as novel insights into the field of TLE. Particularly, in MRI-/PET+ TLE, neurite density imaging may have higher sensitivity than other dMRI parameters. The results may also contribute to better understanding of the pathophysiology of TLE with HS.

1. Introduction

Epilepsy is a common neurological disease affecting approximately 50 million individuals worldwide (Leonardi and Ustun, 2002). Despite advances in antiepileptic drugs (AEDs) since the last century, over 30% of adult patients still have refractory seizures (Loscher and Schmidt, 2011). In current clinical practice, neurosurgical treatment is a widely performed option for such pharmacoresistant epilepsy (Rathore and Radhakrishnan, 2015).

Temporal lobe epilepsy (TLE) is the most common type of adult epilepsy (Engel Jr., 1996). It often shows pharmacoresistance but a relatively favorable response to surgical resection (Wiebe et al., 2001). Hippocampal sclerosis (HS), which is characterized by neuronal loss in the Ammon's horn, astrogliosis, or granule cell dispersion, is considered the most frequent pathology and etiology in TLE (Cendes et al., 2014). Whereas HS can often be detected visually on clinical MRI (Cendes

Abbreviations: AEDs, Anti-epileptic drugs; TLE, Temporal lobe epilepsy; HS, Hippocampal sclerosis; FDG-PET, ^{18}F-fluorodeoxyglucose positron emission tomography; MRI-/PET+, MRI-negative/PET-positive; dMRI, Diffusion MRI; NODDI, Neurite orientation dispersion and density imaging; ICVF, Intracellular volume fraction; ODI, Orientation dispersion index; RSI, Restriction spectrum imaging; FA, Fractional anisotropy; MD, MEAN DIFFUSIVITY; EEG, Electroencephalogram; FSL, FMRIB Software Library; SPM, Statistical parametric mapping; DARTEL, Diffeomorphic anatomical registration using the exponentiated lie; TBSS, Tract-based spatial statistics; ROI, Region of interest; JHU, Johns Hopkins University

* Corresponding author at: National Center of Neurology and Psychiatry, 4-1-1 Ogawa-Higashi, Kodaira, Tokyo 187-8551, Japan.
E-mail address: daichisone@gmail.com (D. Sone).

https://doi.org/10.1016/j.nicl.2018.09.017
Received 24 May 2018; Received in revised form 12 September 2018; Accepted 20 September 2018
Available online 23 September 2018

Table 1
Clinical demographics of patients with TLE and healthy controls.

	Left vs right comparison				Etiology-specific comparison			
	L-TLE (n = 16)	R-TLE (n = 17)	Controls (n = 33)	p	TLE-HS (n = 14)	MRI-/PET+ TLE (n = 19)	Controls (n = 33)	p
Age at examination (years)								
Mean ± SD	40.5 ± 12.2	43.1 ± 11.5	42.1 ± 9.2	0.78[a]	45.6 ± 12.5	39.0 ± 10.5	42.1 ± 9.2	0.20 [a]
Sex (no.)								
Men:women	9:7	6:11	13:20	0.42[b]	6:8	9:10	13:20	0.85 [b]
Laterality (no.)								
Focus side (L:R)	N/A	N/A	N/A	N/A	5:9	11:8	N/A	0.36 [c]
Etiology (no.)								
HS:MRI-PET+	5:11	9:8	N/A	0.36 [c]	N/A	N/A	N/A	N/A
Disease duration (years)								
Mean onset age ± SD	20.3 ± 10.1	18.4 ± 14.2	N/A	0.66 [d]	15.5 ± 10.7	22.1 ± 12.8	N/A	0.13 [d]
Mean duration ± SD	20.3 ± 17.4	24.7 ± 11.4	N/A	0.39 [d]	30.1 ± 13.7	16.9 ± 12.8	N/A	< 0.05 [d]
Current treatment (no.)								
Mean no. of AEDs ± SD	2.38 ± 0.96	2.12 ± 0.93	N/A	0.44[d]	2.43 ± 0.94	2.11 ± 0.94	N/A	0.34 [d]
Seizure types (no.)								
Patients with aura	7	9	N/A	0.86[c]	9	7	N/A	0.23 [c]
Patients with sGTCs	3	4	N/A	0.93[c]	5	2	N/A	0.19 [c]

sGTCs, secondarily generalized tonic-clonic seizures.
[a] One-way ANOVA.
[b] Pearson's χ^2 test.
[c] Pearson's χ^2 test with Yates's correction
[d] Unpaired t-test.

et al., 2014), TLE may show no visual abnormality on MRI (i.e., MRI-negative TLE). However, even in MRI-negative TLE, ^{18}F-fluorodeoxyglucose positron emission tomography (FDG-PET) can detect the focus lesion as a glucose hypometabolic area (Chassoux et al., 2010), and MRI-negative/PET-positive (MRI-/PET+) TLE is also regarded as an important group with favorable surgical outcomes (Kuba et al., 2011; Lopinto-Khoury et al., 2012). Although FDG-PET is a highly useful examination with a sensitivity of 85%–90% for TLE (Kumar and Chugani, 2013), there is still a need for a more advanced methodology for focus detection considering the limited availability and high cost of PET and the inherent radiation exposure.

Recent advances in diffusion MRI (dMRI) have allowed the visualization of more detailed brain microstructures such as neurites (Zhang et al., 2012) and myelin tissues (Fujiyoshi et al., 2016). In particular, neurite orientation dispersion and density imaging (NODDI), which can evaluate neurite density as the intracellular volume fraction (ICVF) and neurite dispersion as the orientation dispersion index (ODI) (Zhang et al., 2012), is expected to contribute to the understanding and localization of focal epilepsy (Winston, 2015) because decreased neurite density has been found in MRI-visible focal cortical dysplasia (Winston et al., 2014). The applications of NODDI to idiopathic epilepsy or neurodegenerative diseases are also reported (Kamagata et al., 2016; Sone et al., 2018). Additionally, Loi and colleagues (Loi et al., 2016) showed reduced neurite density in left and right TLE, mixing both TLE with HS and MRI-negative TLE, by using restriction spectrum imaging (RSI). Decreased neurite density was also suggested to correlate with executive dysfunction in TLE (Reyes et al., 2018). On the other hand, clinical NODDI studies in TLE are still limited, except for a more experimental application study (Lemkaddem et al., 2014). To detect possible abnormalities in neurite density and dispersion in TLE with HS and MRI-/PET+ TLE, we considered that an etiology-specific NODDI application in TLE would provide significant clinical and pathophysiological information to this field.

The aims of this whole-brain voxel-wise statistical neuroimaging study were the following: (1) to confirm and demonstrate neurite density and dispersion in left and right TLE using NODDI, (2) to investigate etiology-specific findings (i.e., TLE with HS and MRI-/PET+ TLE), (3) to compare these findings with conventional dMRI parameters [i.e., fractional anisotropy (FA) and mean diffusivity (MD)], and (4) to explore the correlations of these dMRI metrics with disease duration.

2. Material and methods

2.1. Participants

We recruited 33 patients with TLE (18 females, 15 males; mean ± SD age: 41.8 ± 11.7 years) at our institute between November 2016 and November 2017. TLE was diagnosed based on the presence of focal seizures consistent with TLE and focal epileptiform discharge predominantly in temporal areas on a conventional scalp electroencephalogram (EEG).

Of the 33 patients, unilateral HS was found on conventional MRI in 14 (the TLE-HS group), whereas the other 19 visually showed ipsilateral glucose hypometabolism in interictal FDG-PET and no abnormalities on conventional MRI (the MRI-/PET+ group). Visual assessment of the MRI was performed by experienced neuroradiologists, and the visual diagnostic criteria for HS were the following: ipsilateral reduced hippocampal volume, increased T2 signal in the hippocampus, and abnormal morphology (i.e., a loss of internal architecture of the stratum radiatum, the thin layer of white matter that separates the dentate nucleus and Ammon's horn). Hypometabolism of the ipsilateral temporal lobe was visually diagnosed by a nuclear medicine specialist based on left–right differences.

Clinical data were also reviewed and included seizure onset age, duration of disease, seizure semiology, AEDs, long-term video-EEG monitoring, surgical treatments, and histopathology. The detailed clinical demographics of the groups are shown in Table 1 and in the Results section.

Patients with the following criteria were excluded: a significant medical history of acute encephalitis, meningitis, severe head trauma, or ischemic encephalopathy; suspicious epileptogenic lesions (e.g., tumor, cortical dysplasia, or vascular malformation) on MRI other than ipsilateral HS; contradictory lateralization of focus among MRI, FDG-PET, and long-term video-EEG monitoring; or epileptic paroxysms in extratemporal regions on EEG.

As controls, we also recruited 33 healthy age-matched adults with

no history of neurological or psychiatric disease and no central nervous system medication. All participants gave written informed consent. The study was approved by the Institutional Review Board at the National Center of Neurology and Psychiatry Hospital.

2.2. MRI acquisition

MRI for all patients was performed on a 3.0-Tesla MR system with a 32-channel coil (Philips Medical Systems, Best, The Netherlands). The sequences and their parameters were as follows: three-dimensional (3D) sagittal T1-weighted magnetization prepared rapid acquisition with gradient echo (MPRAGE) images [repetition time (TR)/echo time (TE), 7.18 ms/3.46 ms; flip angle, 10°; number of excitations (NEX), 1; 0.6-mm effective slice thickness with no gap; 300 slices; matrix, 384 × 384; field of view (FOV), 26.1 × 26.1 cm; acquisition time, 4.01 min]; diffusion-weighted images [TR/TE, 6807 ms/87 ms; flip angle, 90°; NEX, 1; voxel dimension of 2.5 × 2.5 × 2.5 mm^3; 60 slices; matrix, 96 × 96; FOV, 24 × 24 cm; acquisition time, 7.36 min]. Diffusion was measured along 32 noncollinear directions at two b-values (1000 and 2000 s/mm^2), and one image was acquired without the use of any diffusion gradient.

We also added a routine MRI examination for TLE with the following sequences: high-resolution T2-weighted images [TR/TE, 6000/78 ms; flip angle, 90°; NEX, 2; 0.43 × 0.43 mm^2 in-plane resolution; 2 mm slice thickness with no gap; 32 slices; matrix, 476 × 377; FOV, 22 × 24 cm; acquisition time, 6.00 min]; sagittal 3D fluid-attenuated inversion recovery (FLAIR) images [TR/TE, 4700/283 ms; inversion time, 1600 ms; NEX, 2; thickness, 0.55 mm with no gap; 340 slices; matrix, 512 × 465; FOV, 26 × 23.4 cm; acquisition time, 5.34 min]. 3D FLAIR images were resliced to 1 mm in axial and coronal orientations.

2.3. Calculations of dMRI parameters

We performed a voxel-based whole brain comparison for NODDI and conventional dMRI parameters. After eddy current correction (i.e., eddy_correct) and brain extraction with FMRIB Software Library (FSL) version 5.0.8 (Smith et al., 2006), the NODDI model was fitted using the NODDI toolbox (https://www.nitrc.org/projects/noddi_toolbox/) running on MATLAB (MathWorks, Natick, MA, USA), and then the ICVF and ODI value maps were calculated. Additionally, we calculated conventional dMRI parameters (i.e., FA and MD) with the diffusion images with b = 1000 s/mm^2. The FA and MD maps were created using the DTIfit command of FSL (ordinary least squares estimation).

To remove extraparenchymal noise, we masked the dMRI parameter maps by the binary mask image. Each individual 3D-T1 image was coregistered and resliced to its b = 0 image, and the coregistered 3D-T1 image was segmented to the gray and white matter images by Statistical Parametric Mapping 12 (SPM12; http://www.fil.ion.ucl.ac.uk/spm/) software running in MATLAB. Then, we created the binary images from their gray and white matter images and masked the dMRI images with the binary image. We visually confirmed the validity of coregistrations between dMRI images and the binary masks.

2.4. Spatial normalization

To investigate the dMRI parameters by whole-brain voxel-wise analyses, these images were spatially normalized using the DARTEL (diffeomorphic anatomical registration using the exponentiated lie) method (Ashburner, 2007) and SPM12. Each individual 3D-T1 image was coregistered and resliced to its b = 0 image, and then the coregistered 3D-T1 image was normalized with DARTEL. Subsequently, the transformation matrix was applied to the dMRI metric maps (i.e., ICVF, ODI, FA, and MD images). Finally, all images were smoothed with a 4-mm full-width at half-maximum (FWHM) Gaussian kernel.

The overall MRI processing methodology was the same as in our previous study of NODDI (Ota et al., 2018), except for the use of SPM12 instead of SPM8. We decided to use SPM12 due to its potential advances over previous versions.

2.5. Focus-unified images for etiology-specific analysis

For etiology-specific analyses (i.e., TLE-HS and MRI-/PET+), we aimed to evaluate ipsilateral and contralateral differences. To analyze the left and right TLE patients together, images of left TLE patients were left–right flipped to make the right hemisphere the ipsilateral hemisphere by using simple imaging software (MRIcro software; http://www.mccauslandcenter.sc.edu/crnl/mricro) before the spatial normalization process. To mitigate the possible left/right bias in the analyses, the control images were also flipped randomly in the same proportions (48%). This left–right flipping process has sometimes been used for unilateral focal epilepsy analysis (Campos et al., 2015; Sone et al., 2016a).

2.6. Hippocampal volumetry and gray matter morphometry

To complement the visual diagnosis of HS on MRI, we performed hippocampal volumetry using FreeSurfer software (version 6.0, https://surfer.nmr.mgh.harvard.edu) based on 3D-T1 images of all the participants. We reported raw hippocampal volumes, total intracranial volumes (TIV), hippocampal volumes corrected for TIV, and laterality index which was calculated by the following formula: (left hippocampus - right hippocampus)/(left hippocampus + right hippocampus).

Additionally, to detect gray matter differences between the groups, we also performed gray matter voxel-wise comparisons using SPM12. The 3D-T1 images of all subjects were segmented and spatially normalized by DARTEL. For an etiology-specific analysis, images of patients and healthy subjects, described in the Section 2.5., were left-right flipped before normalization. All spatially-normalized 3D-T1 images were smoothed with a 4-mm FWHM Gaussian kernel.

2.7. Tract-based spatial statistics

Since the abnormal areas included gray matters on visual inspection of NODDI, such as the hippocampus, we used the whole-brain voxel-wise SPM12 comparison as main analysis. However, considering the potential significance of distortion of dMRI, we also performed tract-based spatial statistics (TBSS) for analysis of white matter tracts. In addition, we evaluated the relationships between FA and ICVF for each group.

To perform three-group comparisons and correlation analysis between FA and ICVF, we adopted an atlas-based region of interest (ROI) analysis using the Johns Hopkins University (JHU) atlas (Wakana et al., 2007). The FA, MD, ICVF, and ODI images of all subjects were skeletonized by TBSS and applied to the JHU atlas. Then, mean values of FA, MD, ICVF, or ODI were calculated within ROIs for the following relevant tracts: forceps major, forceps minor, cingulum (cingulate and hippocampal parts), uncinate fasciculus, inferior fronto-occipital fasciculus, and inferior longitudinal fasciculus.

2.8. Statistical analysis

To reveal dMRI/NODDI abnormalities in left and right TLE, we performed whole-brain voxel-wise comparisons among the three groups (i.e., left TLE vs right TLE vs controls). We applied the normalized dMRI images to the “One-way ANOVA” design of SPM12 with age and sex as nuisance covariates and evaluated the differences in each left and right TLE group from controls by *F*-contrast and post-hoc *T*-contrast estimates.

For etiology-specific comparisons, the focus-unified TLE images (i.e., those with all right-sided focus) and randomly flipped control images were used for the “One-way ANOVA” design (i.e., TLE-HS vs

MRI-/PET+ vs controls) with age and sex as nuisance covariates.

Correlations with disease duration were estimated using the "Multiple regression" design of SPM12 with age and sex as nuisance variables. These correlation analyses were performed separately for each left TLE, right TLE, focus-unified TLE-HS, and focus-unified MRI-/PET + group.

A group comparison of gray matter morphometry was also performed in both left-right and etiology-specific comparisons using "One-way ANOVA" design with age and sex as nuisance covariates.

For all SPM analyses, only results that met the following criteria were deemed significant: a seed threshold of $p < 0.001$ (uncorrected) and an extent threshold of $p < 0.001$ [family-wise error (FWE)].

Clinical were analyzed by SPSS software, version 23.0 (SPSS Japan, Tokyo), using one-way ANOVA, unpaired *t*-test, and Pearson's χ^2 test. The details are shown in Table 1. Additionally, TBSS parameters (i.e. mean FA, MD, ICVF, and ODI values in each tract) were also compared among the three groups, both left-right and etiology-specific, using SPSS, analysis of covariance (ANCOVA) with age and sex as nuisance covariates and Bonferroni correction. For the etiology-specific comparison, the TBSS parameters were left-right flipped in patients with left TLE and healthy subjects, as described in the Section 2.5. To evaluate the relationships between FA and ICVF, we performed a partial correlation analysis for each tract with age and sex as nuisance covariates. For statistics by SPSS, $p < 0.05$ was deemed significant.

3. Results

3.1. Clinical demographics and visual inspection of NODDI

The demographic characteristics of our participants based on both left–right and etiology-specific comparisons are shown in Table 1. There were no significant differences in age, sex, onset age, number of AEDs, and seizure types. The TLE-HS group had a longer disease duration than the MRI-/PET+ group. Of the 33 patients, 19 underwent long-term video-EEG monitoring and 10 underwent surgical resection. Histopathologically, HS was confirmed in all seven patients in the TLE-HS group with surgery, whereas one gliosis and two focal cortical dysplasias were found in the MRI-/PET+ group.

Moreover, nine of 14 patients with TLE-HS and two of 19 patients with MRI-/PET+ TLE showed inter-ictal epileptiform discharges, predominantly in the anterior temporal area on scalp EEG, whereas in the remaining patients epileptiform discharges were found in the middle temporal areas. This difference was statistically significant ($p < 0.05$, Pearson's χ^2 test). As for aura semiology, in the TLE-HS group seven of 14 patients presented with uncomfortable sensations, one with déjà vu, and one with nausea. On the other hand, six of the 19 patients in the MRI-/PET+ group reported auras including uncomfortable sensations, unpleasant smell, cessation of thoughts, dysphagia, nausea, twitching of the contralateral corner of mouth, or ictal fear.

Fig. 1 shows examples of the abnormalities seen on visual inspection of NODDI. One patient with left TLE (MRI-/PET+) showed decreased neurite density in the left temporal tip (Fig. 1-A), whereas another patient with right TLE and HS showed decreased neurite density and dispersion mainly in the hippocampus (Fig. 1-B).

3.2. Voxel-wise comparisons among left TLE, right TLE, and controls

The results of dMRI comparisons among left TLE, right TLE, and controls are shown in Table 2 and Fig. 2. Compared with the controls, the left TLE group presented significant ICVF (i.e., neurite density) reductions and MD increases in the ipsilateral temporal lobe, but no significant FA changes. The right TLE group also showed significant ipsilateral temporal ICVF and MD changes, but these changes were more widespread and severe. Additionally, broad FA decreases were found in the right TLE group. On the other hand, there were no ODI changes in any comparisons. Because the right TLE showed widespread abnormalities, detailed whole-brain figures of the ICVF, FA, and MD changes in this group are shown in Supplementary Fig. S1.

3.3. Voxel-wise comparisons among TLE-HS, MRI-/PET+, and controls

The results of etiology-specific comparisons are presented in Table 3 and Fig. 3. The TLE-HS group showed significantly decreased ICVF and FA and increased MD in broad areas with dominance of the ipsilateral temporal lobe. Notably, a significant reduction in ODI strictly localized to the ipsilateral hippocampus was found in TLE-HS. On the other hand, MRI-/PET+ showed a significant ICVF decrease localized to the ipsilateral temporal pole, with no significance for ODI, FA, and MD. Due to the widespread changes, detailed whole-brain figures of the ICVF, FA, and MD changes in TLE-HS are shown in Supplementary Fig. S2.

3.4. Voxel-wise regression with disease duration

There were two significant results in the regression analyses (Table 4 and Fig. 4). For disease duration, a negative correlation with ipsilateral temporal lobe ICVF was found in the left TLE group, whereas there was a positive correlation with the splenial FA in the TLE-HS group.

3.5. Hippocampal volumetry and gray matter morphometry

The results of hippocampal volumetry are shown in Table 5. Basically, patients with HS showed ipsilateral volume reduction of the hippocampus. Fig. 5 presents the comparison of laterality indices of hippocampal volumes; the laterality indices within each group appeared consistent with the visual diagnosis.

Additionally, we also report whole-brain gray matter comparisons. Compared with the controls, the right TLE group showed significant gray matter reduction in the right hippocampus, whereas more profound gray matter reduction in the ipsilateral hippocampus was found in the TLE-HS group. There were no significant differences for the other comparisons with controls.

3.6. Atlas-based ROI analysis in TBSS

The results of left-right and etiology-specific comparisons in the atlas-based ROI analysis are shown in Tables 6 and 7, respectively. The right TLE and the TLE-HS groups presented with widespread abnormal areas in FA, MD, and ICVF, whereas the MRI-/PET+ TLE showed small abnormalities mainly in the ipsilateral uncinate fasciculus. Though these results were generally consistent with the voxel-wise comparisons, the mean FA and MD as well as ICVF values showed abnormal in the MRI-/PET+ TLE.

Moreover, we evaluated the relationships between FA and ICVF in each tract. The results of partial correlation analysis are shown in Table 8. For the controls, we observed positive correlations for most tracts except cingulum, which was also observed in patients with TLE. However, in the TLE-HS we did not find significant correlations for the ipsilateral uncinate fasciculus and bilateral inferior longitudinal fasciculus tracts. On the other hand, the MRI-/PET+ TLE showed a significant positive correlation for the ipsilateral cingulate gyrus, which was not seen in controls.

4. Discussion

In the current study, we investigated NODDI findings as well as conventional dMRI parameters in patients with TLE with and without HS. We found decreased neurite density mainly in the ipsilateral temporal areas of both right and left TLE, with right TLE showing more severe and broad abnormalities (Fig. 2). In addition, our etiology-specific analyses revealed a localized reduction in neurite density in the ipsilateral temporal pole in MRI-/PET+ TLE, whereas TLE with HS

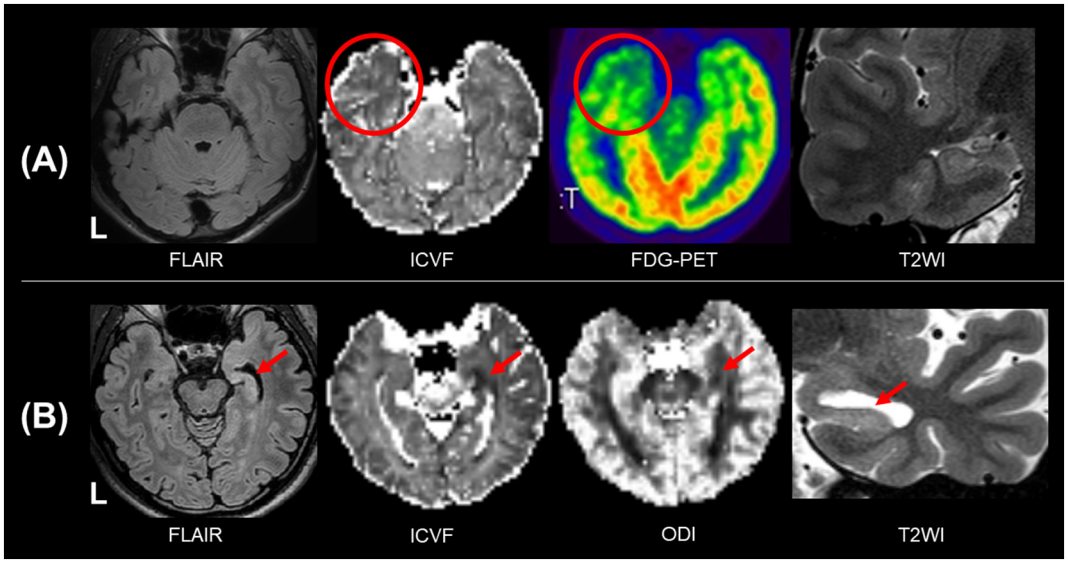

Fig. 1. Examples of neurite density and dispersion imaging at our institute. (A) MRI-/PET+ left TLE shows decreased neurite density in the left temporal tip (circles). (B) Right TLE with HS shows decreased neurite density and dispersion mainly in the hippocampus (arrows).

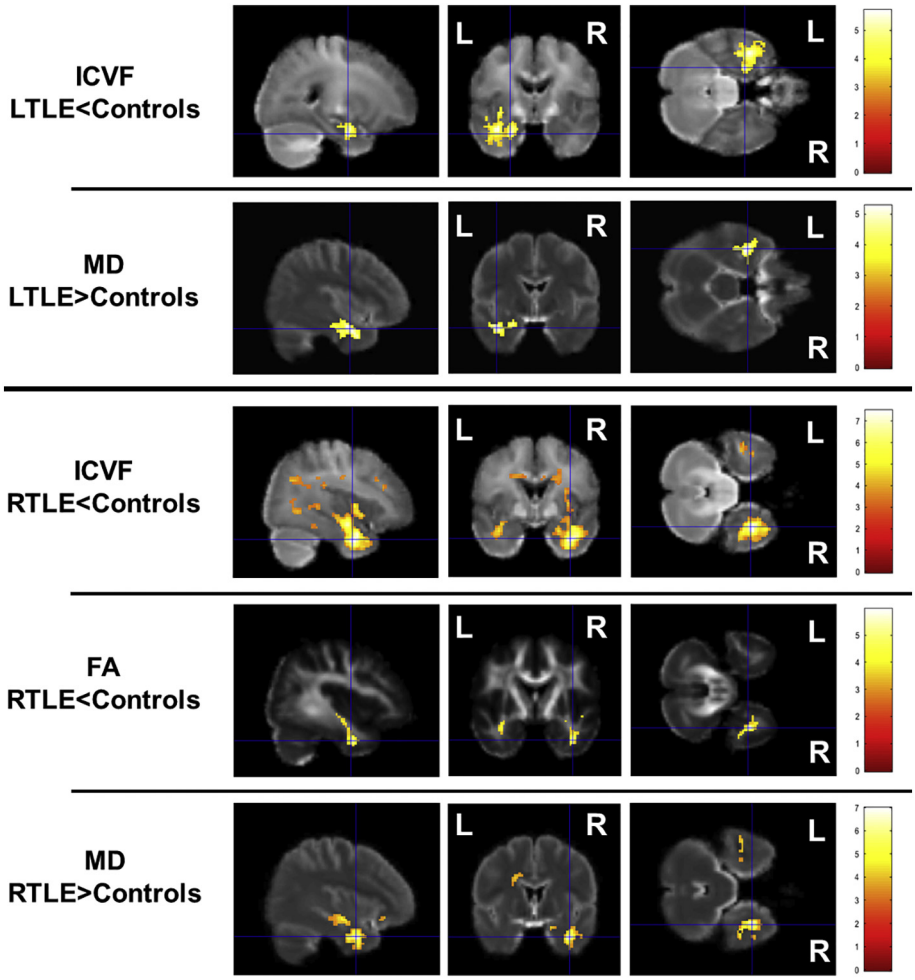

Fig. 2. Results of dMRI comparisons among left TLE, right TLE, and controls. R: right, L: left. The color bars denote *T*-values. All clusters were significant at the following levels: a seed threshold of $p < 0.001$ (uncorrected) and a cluster extent threshold of $p < 0.001$ (FWE). Detailed whole-brain figures of the ICVF, FA, and MD changes in right TLE are shown in Supplementary Fig. S1.

presented greater abnormalities, including FA and MD, in addition to a localized hippocampal reduction in neurite dispersion (Fig. 3). In particular, in MRI-/PET+ TLE, neurite density imaging may provide higher sensitivity than other dMRI parameters, although the abnormalities were less severe than those of TLE with HS. As for TLE with HS, our findings may contribute to better understanding of the pathophysiology.

A number of articles have been published on conventional dMRI findings in TLE with and without HS (Campos et al., 2015; Concha et al., 2009; Otte et al., 2012; Sone et al., 2016b). It has been relatively

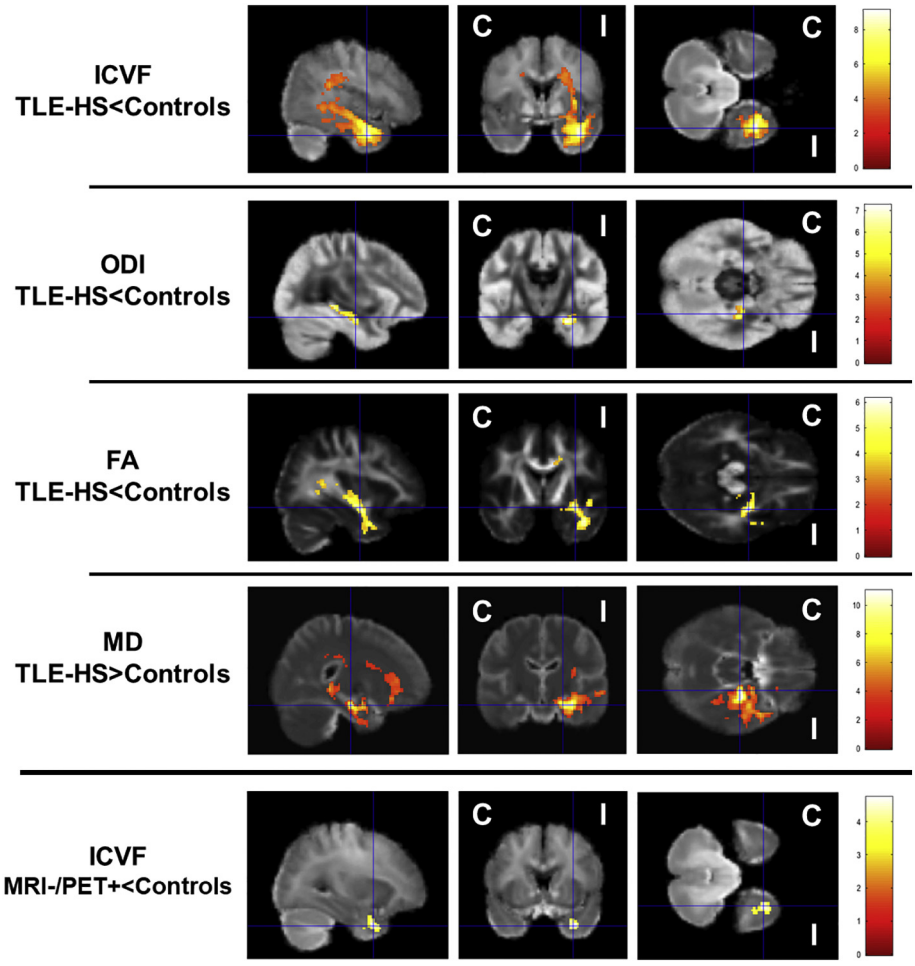

Fig. 3. Results of dMRI comparisons among TLE-HS, MRI-/PET+, and controls. I: ipsilateral, C: contralateral. The color bars denote *T*-values. All clusters were significant at the following levels: a seed threshold of $p < 0.001$ (uncorrected) and a cluster extent threshold of $p < 0.001$ (FWE). Due to the widespread changes, detailed whole-brain figures of the ICVF, FA, and MD changes in TLE-HS are shown in Supplementary Fig. S2.

Table 2
Significant voxel-wise differences in dMRI/NODDI parameters among left TLE, right TLE, and controls.

Analysis	Parameter	Cluster size	*T*-val.	x	y	z	Regions of peaks
Left TLE							
Controls > Left TLE	ICVF	949	5.69	−25	−8	−21	Lt. PHG
Left TLE > Controls	MD	330	5.26	−39	−6	−18	Lt. TL-sub
Right TLE							
Controls > Right TLE	ICVF	4162	**7.47**	**36**	**−4**	**−24**	**Rt. TL-sub, PHG**
		284	5.31	−36	−8	−12	Lt. TL-sub
Controls > Right TLE	FA	115	**5.95**	**−19**	**−51**	**29**	**Lt. PCUN**
		384	**5.60**	**38**	**−7**	**−26**	**Rt. TL-sub, ITG**
		349	5.28	4	29	−1	Rt. ACG[a]
		125	5.17	15	−31	27	Rt. PCG, CC
		183	5.00	−45	−12	−5	Rt. STG[a]
Right TLE > Controls	MD	689	**6.97**	**36**	**−1**	**−24**	**Rt. TL-sub, PHG**
		359	**5.67**	**−22**	**26**	**0**	**Rt. FL-sub**
		376	5.30	7	29	−1	Rt. ACG, CC
		119	4.63	2	−19	−4	Rt. Mid
		166	4.57	−24	−48	23	Lt. PL-sub
		96	4.42	−38	−11	−27	Lt. ITG

All clusters are significant at seed $p < 0.001$ (uncorrected) and extent $p < 0.001$ (FWE correction). Bold font denotes seed $p < 0.05$ (FWE correction). Coordinates are shown for the TalairachAtlas.

TL, temporal lobe; FL, frontal lobe; PL, parietal lobe; −sub, subgyral white matter; ACG, anterior cingulate gyrus; CC, corpus callosum; PCG, posterior cingulate gyrus; PHG, parahippocampal gyrus; ITG, inferior temporal gyrus; STG, superior temporal gyrus; PCUN, precuneus; Mid, midbrain; Lt, left; Rt, right.

[a] Denotes gray matter, and all other peak regions are white matter.

consistently reported that TLE with HS shows more extensive abnormalities than MRI-negative TLE in both volumetric studies (Campos et al., 2015; Mueller et al., 2006) and conventional dMRI analyses (Campos et al., 2015; Concha et al., 2009). Our NODDI results would support these findings in that more extensive damage was suggested in TLE with HS. In accordance with our results, a previous neurite imaging study of TLE using another advanced dMRI analysis (i.e., RSI) also reported a prominent neurite density reduction in the ipsilateral temporal

Table 3
Significant voxel-wise differences in dMRI/NODDI parameters among TLE-HS, MRI-/PET+, and controls.

Analysis	Parameter	Cluster size	*T*-val.	x	y	z	Regions of peaks
TLE-HS							
Controls > TLE-HS	ICVF	4249	**9.11**	**41**	**−2**	**−24**	**Ipsi. TL-sub, FG**
		351	4.54	−8	31	3	Contra. ACG, CC
Controls > TLE-HS	ODI	176	**7.23**	**24**	**−12**	**−16**	**Ipsi. Hip[a], PHG**
Controls > TLE-HS	FA	1147	**6.14**	**33**	**−8**	**−9**	**Ipsi. TL-sub**
		470	**5.98**	**17**	**18**	**31**	**Ipsi. ACG**
		150	5.14	−19	−38	36	Contra. PCG
TLE-HS > Controls	MD	2075	**11.00**	**22**	**−17**	**−13**	**Ipsi. PHG**
		382	**5.50**	**24**	**31**	**−2**	**Ipsi. IFG**
		124	4.77	−22	26	2	Contra. FL-sub
		143	4.56	37	−28	12	Ipsi. TTG
MRI-/PET+							
Controls > MRI-/PET+	ICVF	166	4.73	32	4	−29	Ipsi. TL-sub

All clusters are significant at seed $p < 0.001$ (uncorrected) and extent $p < 0.001$ (FWE correction). Bold font denotes seed $p < 0.05$ (FWE correction).
Coordinates are shown for the Talairach Atlas.
TL, temporal lobe; FL, frontal lobe; −sub, subgyral white matter; ACG, anterior cingulate gyrus; CC, corpus callosum; PCG, posterior cingulate gyrus; PHG, parahippocampal gyrus; FG, fusiform gyrus; TTG, transverse temporal gyrus; Hip, hippocampus; Ipsi, ipsilateral; Contra, contralateral.
[a] denotes gray matter, and all other peak regions are white matter.

Table 4
Significant voxel-wise regressions of dMRI/NODDI parameters with disease duration in each TLE group.

Analysis	Parameter	Cluster size	*T*-val.	x	y	z	Regions of peaks
Left TLE							
Negative correlation	ICVF	73	8.04	−53	−4	−17	Lt. MTG[a]
TLE-HS							
Positive correlation	FA	88	8.27	−4	−34	15	Contra. CC

All clusters are significant at seed $p < 0.001$ (uncorrected) and extent $p < 0.001$ (FWE correction).
Coordinates are shown for the Talairach Atlas.
MTG, middle temporal gyrus; CC, corpus callosum; Lt, left; Contra, contralateral.
[a] denotes gray matter and the other peak is white matter.

lobe in mixed patients of TLE with HS and MRI-negative TLE (Loi et al., 2016). We speculate that the current study would provide meaningful knowledge to this field by revealing the different neurite imaging patterns between TLE with HS and MRI-negative TLE.

Indeed, MRI-/PET+ TLE constitutes a highly important patient group in clinical practice because it has a favorable postsurgical seizure outcome that is comparable with that of TLE with HS (Lopinto-Khoury et al., 2012). The most common histopathology of MRI-/PET+ TLE is cortical dysplasia (Kuba et al., 2011), and the initial NODDI application study of epilepsy revealed decreased neurite density in MRI-positive cortical dysplasia (Winston et al., 2014). Thus, our results of reduced neurite density in MRI-/PET+ TLE would be concordant with these past findings. Additionally, our MRI-/PET+ group showed no significant results for the other parameters, and the neurite density parameter may have higher sensitivity than conventional dMRI analyses, as suggested (Winston et al., 2014; Loi et al., 2016). On the other hand, in terms of histopathology, our MRI-/PET+ group contained a patient with gliosis in addition to two patients with cortical dysplasia. Additionally, the detailed focus locations in this group would not necessarily be the same region within the temporal lobe, although the temporal pole, where the ICVF reduction was localized, is one of the most common ictal focuses in MRI-/PET+ TLE (Kuba et al., 2011). Thus, although we called this group analysis “etiology-specific”, the MRI-/PET+ TLE group possibly did display heterogeneity, as the variability of aura semiology suggests. Especially, given the greater number of patients with middle temporal discharges on EEG, the MRI-/PET+ group may likely represent patients with neocortical TLE. At any rate, although clinicians have to detect MRI-/PET+ TLE to identify surgical candidates, the availability of PET is still limited, particularly in developing countries (Kashyap et al., 2013). In this context, it would be meaningful to reveal the potential of NODDI as a novel biomarker beyond conventional dMRI metrics in MRI-/PET+ TLE.

In addition, we found a severe but localized reduction in neurite dispersion in the ipsilateral hippocampus in TLE with HS. Notably, this

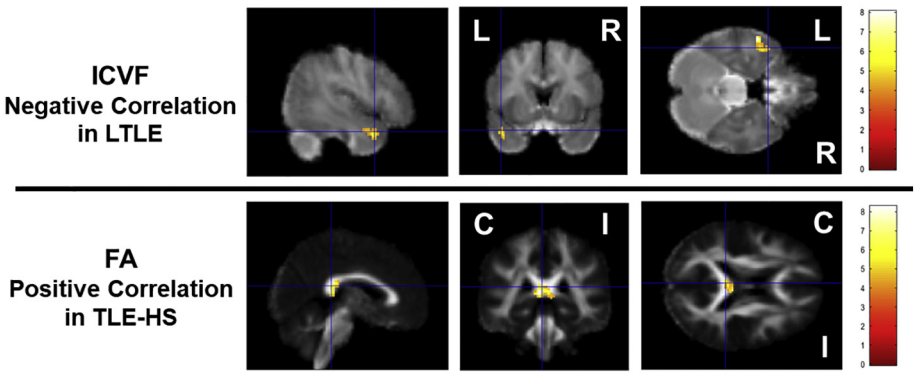

Fig. 4. Results of regression analyses between dMRI metrics and disease duration in each TLE group. R: right, L: left, I: ipsilateral, C: contralateral. The color bars denote *T*-values. All clusters were significant at the following levels: a seed threshold of $p < 0.001$ (uncorrected) and a cluster extent threshold of $p < 0.001$ (FWE).

Table 5
Mean ± SD and ranges of hippocampal volumes, TIV, and laterality index in each group.

	Left TLE HS	Left TLE MRI-/PET+	Right TLE HS	Right TLE MRI-/PET+	Controls
TIV (mm^3) × 10^{-6}	1.50 ± 0.20 [1.33–1.77]	1.50 ± 0.26 [1.03–1.85]	1.44 ± 0.21 [1.16–1.70]	1.42 ± 0.31 [0.93–1.76]	1.46 ± 0.23 [1.00–1.81]
Left Hip (mm^3)	3380 ± 388 [2930–3910]	4863 ± 545 [4188–5850]	4605 ± 331 [4040–5209]	4310 ± 397 [3643–4760]	4498 ± 443 [3720–5434]
Left Hip (mm^3) × 10^6/TIV	2282 ± 345 [1757–2700]	3326 ± 604 [2698–4492]	3267 ± 512 [2662–4114]	3155 ± 623 [2578–3929]	3135 ± 427 [2448–4058]
Right Hip (mm^3)	4475 ± 431 [3858–4952]	4786 ± 485 [4120–5740]	3420 ± 447 [2734–4184]	4542 ± 578 [3812–5245]	4559 ± 469 [3662–5304]
Right Hip (mm^3) × 10^6/TIV	3003 ± 217 [2686–3198]	3283 ± 614 [2329–4415]	2394 ± 185 [2081–2699]	3305 ± 592 [2607–4094]	3175 ± 420 [2510–4076]
Laterality Index	−0.14 ± 0.046 [−0.21 to −0.08]	0.01 ± 0.035 [−0.05–0.09]	0.15 ± 0.060 [0.06–0.23]	−0.02 ± 0.030 [−0.08–0.02]	−0.01 ± 0.033 [−0.09–0.08]

TIV: total intracranial volumes, Hip: hippocampus.

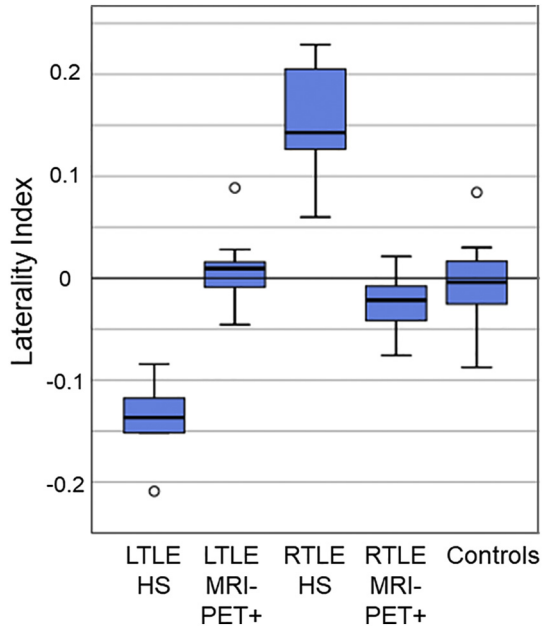

Fig. 5. Boxplot of the laterality index of hippocampal volumes in each group. The calculation method of laterality index is described in the Material and Methods.

finding was not found in extrahippocampal areas (Fig. 3). Interestingly, abnormal branching angles of apical dendrites have been revealed in HS histopathological tissues (Thom, 2014), although their relationship with our findings should be elucidated by further comprehensive studies of dMRI and histopathology, as emphasized by a recent review (Deleo et al., 2018). As for neurite dispersion, the most recent NODDI study of focal epilepsy suggested ODI changes (Rostampour et al., 2018). Given that neurite density has been correlated with executive function (Reyes et al., 2018), neurite dispersion might also be a candidate for future clinical research.

We have also reported comparisons among left TLE, right TLE, and controls. The ipsilateral temporal reduction in neurite density in both left and right TLE was consistent with a previous study of TLE and RSI (Loi et al., 2016). As for the differences between left and right TLE, our results suggested more severe and extensive abnormalities in ICVF, FA, and MD for right TLE than left TLE (Fig. 2). We consider the main reason for this difference to be that the right TLE group contained a greater proportion of TLE with HS patients (Table 1), although the difference in the proportion was not statistically significant ($p = 0.36$). On the other hand, there is still controversy about the differences between left and right TLE. A prior paper on FA in TLE reported a more severe and diffuse FA reduction in left TLE (Ahmadi et al., 2009), whereas a more recent study suggested greater connectivity abnormalities in right TLE than left TLE (Lemkaddem et al., 2014). These studies also analyzed both TLE with HS and MRI-negative TLE as one package. To obtain robust answers to this controversy, a larger multimodal investigation on the basis of etiologies is required.

There were some significant results in the regression analyses. The negative correlation between ICVF and disease duration in left TLE was concordant with previous results (Loi et al., 2016). On the other hand, the positive correlation of disease duration with FA in the corpus callosum was paradoxical and conflicted with previous work (Keller et al., 2012). However, the findings of past papers are also inconsistent regarding the correlations between dMRI metrics and duration of TLE (Loi et al., 2016; Concha et al., 2009; Keller et al., 2012; Chiang et al., 2016). Therefore, the relationships between brain structures and epilepsy duration are still unclear, even in volumetric studies, despite the wealth of published work (Caciagli et al., 2017). More studies would thus be desirable in this field.

We performed hippocampal volumetry using FreeSurfer, as quantitative analysis of hippocampal volumes supports the diagnosis of HS (Coan et al., 2014). Laterality indices within each group were consistent with the visual diagnosis (Fig. 5), and thus, we consider the results complement and validate the classification in this study. On the other hand, gray matter morphometry revealed localized atrophy in the ipsilateral hippocampus only in the right TLE and the TLE-HS groups (Fig. 6). We attribute the lack of significance in the left TLE to the smaller number of patients with HS. According to a recent multi-center study (Whelan et al., 2018), TLE patients with HS generally show more widespread gray matter loss, which appears to differ from the localized hippocampal atrophy in our patients. This discrepancy might be caused by the differences in sample size and methodology used.

Furthermore, to complement the main comparisons, we performed an atlas-based ROI analysis of dMRI parameters within relevant white matter tracts. The degree and extent of abnormalities of each group were generally consistent with the main findings. On the other hand, we found several distinct relationships between FA and ICVF in TLE patients compared to controls: in the TLE-HS group we did not detect correlations between mean FA and ICVF in the tracts associated with temporal lobes, whereas the MRI-/PET+ TLE patients presented with an abnormal positive correlation for the ipsilateral cingulate gyrus (Table 8). The pathological significance of these findings is still unclear and needs to be elucidated in further investigations.

This study has several limitations. First, the sample size was not large and we were thus unable to perform five-group ANOVA analyses (i.e., right TLE-HS, left TLE-HS, right MRI-/PET+, left MRI-/PET+, and controls). The use of an uncorrected p-value for seed-level should be another limitation, but we consider that the FWE-corrected $p < 0.001$ for cluster size could partly overcome this limitation and some of the results showed higher robustness (FWE-corrected $p < 0.05$ at the seed-level). On the other hand, the group-level statistical significance does

Table 6
Results of atlas-based ROI analyses of the relevant tracts in the left-right comparison. Mean ± SD values of each dMRI parameter are shown.

	FA	MD × 10^3	ICVF	ODI	FA	MD × 10^3	ICVF	ODI
	Forceps major				Forceps minor			
Controls	0.67 ± 0.019	0.76 ± 0.023	0.62 ± 0.030	0.12 ± 0.012	0.52 ± 0.020	0.77 ± 0.036	0.52 ± 0.036	0.19 ± 0.016
L-TLE	0.66 ± 0.029	0.76 ± 0.028	0.62 ± 0.032	0.12 ± 0.017	**0.50 ± 0.032** *	0.79 ± 0.037	0.50 ± 0.040	0.19 ± 0.014
R-TLE	**0.64 ± 0.040** ***	0.78 ± 0.033	0.60 ± 0.037	0.13 ± 0.017	**0.48 ± 0.042** ***	**0.82 ± 0.064** **	**0.48 ± 0.052** **	0.19 ± 0.014
	Cingulum (cingulate gyrus) L				Cingulum (cingulate gyrus) R			
Controls	0.53 ± 0.035	0.74 ± 0.036	0.64 ± 0.044	0.19 ± 0.019	0.49 ± 0.037	0.74 ± 0.040	0.64 ± 0.048	0.21 ± 0.025
L-TLE	0.51 ± 0.050	0.76 ± 0.057	0.63 ± 0.046	0.20 ± 0.025	0.48 ± 0.045	0.76 ± 0.054	0.63 ± 0.039	0.22 ± 0.030
R-TLE	**0.50 ± 0.045** *	0.77 ± 0.048	0.62 ± 0.060	0.20 ± 0.023	**0.44 ± 0.049** ***	0.78 ± 0.068	**0.59 ± 0.063** *	**0.24 ± 0.029** *
	Cingulum (hippocampus) L				Cingulum (hippocampus) R			
Controls	0.46 ± 0.043	0.69 ± 0.042	0.58 ± 0.041	0.25 ± 0.033	0.42 ± 0.042	0.72 ± 0.049	0.56 ± 0.048	0.26 ± 0.035
L-TLE	**0.40 ± 0.055** **	0.72 ± 0.074	0.55 ± 0.066	0.27 ± 0.039	0.40 ± 0.049	0.73 ± 0.051	0.54 ± 0.050	0.27 ± 0.037
R-TLE	0.42 ± 0.054	0.70 ± 0.072	0.58 ± 0.057	0.27 ± 0.057	0.39 ± 0.060	**0.75 ± 0.050** *	**0.53 ± 0.054** *	0.27 ± 0.046
	Uncinate fasciculus L				Uncinate fasciculus R			
Controls	0.43 ± 0.030	0.78 ± 0.030	0.50 ± 0.026	0.21 ± 0.014	0.47 ± 0.033	0.79 ± 0.036	0.49 ± 0.033	0.19 ± 0.017
L-TLE	0.41 ± 0.033	**0.82 ± 0.034** **	**0.46 ± 0.032** **	0.21 ± 0.019	0.46 ± 0.044	0.78 ± 0.042	0.48 ± 0.038	0.19 ± 0.017
R-TLE	**0.39 ± 0.042** **	**0.81 ± 0.039** **	**0.46 ± 0.034** **	0.22 ± 0.020	**0.41 ± 0.042** ***	**0.84 ± 0.059** **	**0.45 ± 0.035** ***	**0.21 ± 0.023** **
	Inferior fronto-occipital fasciculus L				Inferior fronto-occipital fasciculus R			
Controls	0.47 ± 0.021	0.78 ± 0.025	0.51 ± 0.026	0.20 ± 0.012	0.47 ± 0.022	0.80 ± 0.035	0.51 ± 0.028	0.20 ± 0.013
L-TLE	**0.45 ± 0.038** **	**0.81 ± 0.036** **	**0.48 ± 0.035** **	0.20 ± 0.016	0.45 ± 0.033	0.80 ± 0.031	0.49 ± 0.029	0.20 ± 0.015
R-TLE	**0.45 ± 0.036** *	**0.82 ± 0.047** **	**0.48 ± 0.041** **	0.20 ± 0.018	**0.44 ± 0.034** ***	0.83 ± 0.038	**0.47 ± 0.039** **	0.21 ± 0.013
	Inferior longitudinal fasciculus L				Inferior longitudinal fasciculus R			
Controls	0.46 ± 0.021	0.78 ± 0.028	0.50 ± 0.029	0.22 ± 0.014	0.46 ± 0.027	0.79 ± 0.034	0.50 ± 0.031	0.21 ± 0.016
L-TLE	0.44 ± 0.041	**0.81 ± 0.042** *	**0.47 ± 0.034** *	0.21 ± 0.021	0.45 ± 0.028	0.79 ± 0.027	0.49 ± 0.026	0.22 ± 0.017
R-TLE	**0.43 ± 0.033** *	0.80 ± 0.045	**0.48 ± 0.037** *	0.22 ± 0.016	**0.44 ± 0.029** *	**0.82 ± 0.037** *	**0.46 ± 0.033** ***	0.21 ± 0.018

Bold font in the mean ± SD values denotes significant difference compared with the controls. * $p < 0.05$, **: $p < 0.01$, ***: $p < 0.001$, R: right, L: left.

Table 7
Results of atlas-based ROI analyses of the relevant tracts in the etiology-specific comparison. Mean ± SD values of each dMRI parameter are shown.

	FA	MD × 10^3	ICVF	ODI	FA	MD × 10^3	ICVF	ODI
	Forceps major				Forceps minor			
Controls	0.67 ± 0.019	0.76 ± 0.023	0.62 ± 0.030	0.12 ± 0.012	0.52 ± 0.020	0.77 ± 0.036	0.52 ± 0.036	0.19 ± 0.016
TLE-HS	**0.63 ± 0.034** ***	0.78 ± 0.033	0.60 ± 0.028	0.13 ± 0.017	**0.48 ± 0.033** ***	**0.82 ± 0.052** *	**0.47 ± 0.044** **	0.19 ± 0.011
MRI+/PET-	0.66 ± 0.033	0.76 ± 0.027	0.62 ± 0.036	0.12 ± 0.016	**0.50 ± 0.038** **	0.80 ± 0.055	0.50 ± 0.048	0.19 ± 0.016
	Cingulum (cingulate gyrus) Ipsi				Cingulum (cingulate gyrus) Contra			
Controls	0.51 ± 0.038	0.74 ± 0.038	0.64 ± 0.050	0.20 ± 0.026	0.51 ± 0.044	0.74 ± 0.038	0.64 ± 0.043	0.20 ± 0.023
TLE-HS	**0.44 ± 0.042** ***	**0.78 ± 0.050** *	**0.59 ± 0.060** *	**0.23 ± 0.025** **	0.49 ± 0.052	0.78 ± 0.047	0.61 ± 0.052	0.20 ± 0.024
MRI+/PET-	0.50 ± 0.058	0.75 ± 0.069	0.62 ± 0.053	0.21 ± 0.032	0.49 ± 0.040	0.75 ± 0.052	0.63 ± 0.049	0.22 ± 0.032
	Cingulum (hippocampus) Ipsi				Cingulum (hippocampus) Contra			
Controls	0.44 ± 0.051	0.70 ± 0.042	0.58 ± 0.040	0.25 ± 0.034	0.44 ± 0.038	0.71 ± 0.052	0.57 ± 0.050	0.26 ± 0.036
TLE-HS	**0.36 ± 0.042** ***	**0.79 ± 0.040** ***	**0.50 ± 0.050** ***	0.28 ± 0.045	0.40 ± 0.050	0.70 ± 0.058	0.57 ± 0.054	0.29 ± 0.047
MRI+/PET-	0.42 ± 0.052	0.70 ± 0.051	0.57 ± 0.053	0.27 ± 0.041	0.42 ± 0.053	0.72 ± 0.067	0.55 ± 0.058	0.26 ± 0.048
	Uncinate fasciculus Ipsi				Uncinate fasciculus Contra			
Controls	0.45 ± 0.038	0.79 ± 0.028	0.49 ± 0.028	0.20 ± 0.020	0.45 ± 0.035	0.78 ± 0.038	0.50 ± 0.031	0.20 ± 0.021
TLE-HS	**0.39 ± 0.032** ***	**0.84 ± 0.045** ***	**0.44 ± 0.029** ***	0.21 ± 0.024	0.41 ± 0.038	0.80 ± 0.034	**0.47 ± 0.029** *	0.21 ± 0.018
MRI+/PET-	**0.42 ± 0.037** **	**0.82 ± 0.050** *	**0.47 ± 0.033** *	0.21 ± 0.019	0.43 ± 0.063	0.80 ± 0.049	0.48 ± 0.042	0.20 ± 0.028
	Inferior fronto-occipital fasciculus Ipsi				Inferior fronto-occipital fasciculus Contra			
Controls	0.47 ± 0.023	0.79 ± 0.031	0.51 ± 0.028	0.20 ± 0.013	0.47 ± 0.020	0.79 ± 0.032	0.51 ± 0.027	0.20 ± 0.012
TLE-HS	**0.42 ± 0.026** ***	**0.84 ± 0.031** ***	**0.45 ± 0.033** ***	0.21 ± 0.013	**0.44 ± 0.027** **	0.82 ± 0.034	**0.48 ± 0.034** **	0.20 ± 0.013
MRI+/PET-	0.46 ± 0.035	0.80 ± 0.032	0.49 ± 0.032	0.20 ± 0.016	0.46 ± 0.037	0.80 ± 0.044	0.49 ± 0.036	0.20 ± 0.019
	Inferior longitudinal fasciculus Ipsi				Inferior longitudinal fasciculus Contra			
Controls	0.46 ± 0.023	0.79 ± 0.032	0.50 ± 0.031	0.21 ± 0.017	0.46 ± 0.025	0.78 ± 0.031	0.50 ± 0.029	0.21 ± 0.014
TLE-HS	**0.42 ± 0.020** ***	**0.84 ± 0.037** ***	**0.44 ± 0.029** ***	0.21 ± 0.019	**0.43 ± 0.023** *	0.80 ± 0.028	**0.47 ± 0.027** *	0.22 ± 0.015
MRI+/PET-	0.45 ± 0.035	0.80 ± 0.032	0.48 ± 0.028	0.21 ± 0.020	0.45 ± 0.033	0.79 ± 0.044	0.49 ± 0.035	0.22 ± 0.018

Bold font in the mean ± SD values denotes significant difference compared with the controls. *: $p < 0.05$, **: $p < 0.01$, ***: $p < 0.001$, Ipsi: ipsilateral, Contra: contralateral.

not necessarily equal individual-based usefulness. For further clinical application, we need to verify these findings at the individual-level. In addition, pathological findings were not available for all patients, which could raise concerns about the heterogeneity of the MRI-/PET+ TLE group. However, FDG-PET has high sensitivity for TLE (Kumar and Chugani, 2013) and this group is regarded as clinically important. Although the potential distortion of images by eddy current of dMRI or the left–right flipping procedure could also be limitations, our results were generally consistent with previous knowledge.

Finally, we must consider the weakness of our NODDI imaging protocol. Given the lower signal-to-noise ratio at higher b-values, the outer shell would typically have a greater number of directions. The single non-diffusion weighted image in our protocol is also an important limitation, considering the large effect on fitted parameters caused by noise. On the other hand, a long acquisition time could prevent the application of NODDI in clinical practice. We speculate our

Table 8
The results of partial correlations between FA and ICVF values in each tract. Partial correlation coefficient is shown.

	Left vs Right Comparison				Etiology-specific Comparison		
	Controls	LTLE	RTLE		Controls	TLE-HS	MRI-/PET+
Forceps							
Major	0.334	**0.757** **	0.391	Major	0.334	0.377	**0.751** **
Minor	**0.653** ***	**0.771** **	**0.789** ***	Minor	**0.653** ***	**0.839** **	**0.814** ***
Cingulum (cingulate gyrus)							
Left	0.150	**0.670** **	0.459	Ipsi	−0.023	0.353	**0.804** ***
Right	0.045	−0.212	0.328	Contra	0.260	0.457	0.020
Cingulum (hippocampus)							
Left	0.344	**0.574** *	0.293	Ipsi	**0.519** **	0.316	0.451
Right	0.349	0.533 *	0.448	Contra	0.289	0.543	0.452
Uncinate fasciculus							
Left	**0.685** ***	**0.596** *	**0.621** *	Ipsi	**0.608** ***	0.389	**0.646** **
Right	**0.682** ***	**0.766** **	**0.621** *	Contra	**0.495** **	**0.671** *	**0.788** ***
Inferior fronto-occipital fasciculus							
Left	0.614 ***	**0.740** **	**0.623** *	Ipsi	**0.579** **	**0.797** **	**0.690** **
Right	**0.566** **	**0.773** **	**0.777** **	Contra	**0.612** ***	**0.590** *	**0.775** ***
Inferior longitudinal fasciculus							
Left	**0.496** **	**0.692** **	**0.566** *	Ipsi	**0.514** **	0.364	**0.562** *
Right	**0.548** **	**0.735** **	**0.619** *	Contra	**0.556** **	0.480	**0.731** **

Bold font in the partial correlation coefficient denotes statistical significance. * $p < 0.05$, **: $p < 0.01$, ***: $p < 0.001$, Ipsi: ipsilateral, Contra: contralateral.

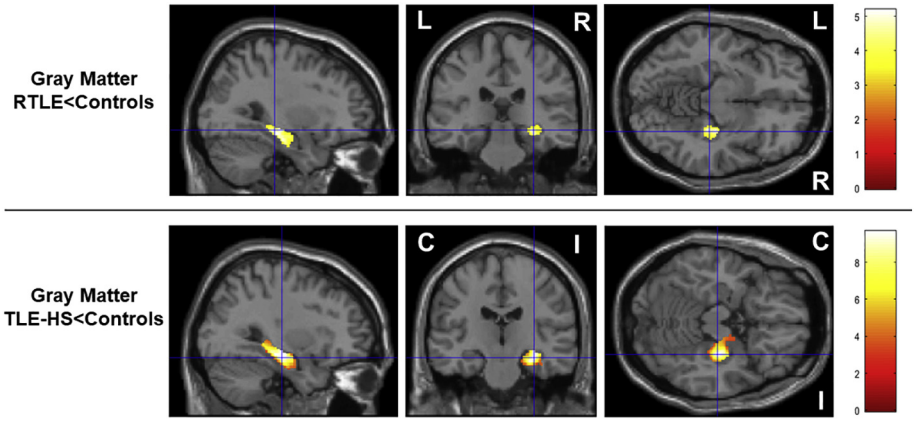

Fig. 6. Results of gray matter volume comparisons in both left-right and etiology-specific comparisons. The other comparisons with the controls had no significant clusters. R: right, L: left, I: ipsilateral, C: contralateral. The color bars denote *T*-values. All clusters were significant at the following levels: a seed threshold of $p < 0.001$ (uncorrected) and a cluster extent threshold of $p < 0.001$ (FWE).

protocol also suggest the clinically acceptable acquisition time of NODDI (i.e. 7.36 min), although the notable limitation of the protocol should be kept in mind.

5. Conclusions

NODDI analyses in TLE showed mainly an ipsilateral temporal reduction in neurite density in both left and right TLE. In particular, MRI-/PET+ TLE showed a localized decrease in neurite density in the ipsilateral temporal pole with no other dMRI abnormalities. TLE with HS presented greater and more extensive abnormalities in neurite density as well as FA and MD, but the severe neurite dispersion reduction was restricted to the ipsilateral hippocampus. We anticipate that the results of this study will be clinically relevant as well as will provide novel insights into the field of TLE.

Supplementary data to this article can be found online at https://doi.org/10.1016/j.nicl.2018.09.017.

Conflicts of interest

None.

Acknowledgements

This study was supported by grants from the Japan Epilepsy Research Foundation (JERF TENKAN 17009) and the Japan Society for the Promotion of Science (KAKENHI Grant Number JP17H07385) (both to DS).

References

Ahmadi ME, Hagler DJ, Jr., McDonald CR, Tecoma ES, Iragui VJ, Dale AM, et al. Side matters: diffusion tensor imaging tractography in left and right temporal lobe epilepsy. AJNR Am. J. Neuroradiol. 2009;30(9):1740–7. Epub 2009/06/11. doi: https://doi.org/10.3174/ajnr.A1650. (PubMed PMID: 19509072; PubMed Central PMCID: PMCPmc2759860).

Ashburner, J., 2007. A fast diffeomorphic image registration algorithm. NeuroImage 38 (1), 95–113. https://doi.org/10.1016/j.neuroimage.2007.07.007. (PubMed PMID: 17761438).

Caciagli, L., Bernasconi, A., Wiebe, S., Koepp, M.J., Bernasconi, N., Bernhardt, B.C., 2017. A meta-analysis on progressive atrophy in intractable temporal lobe epilepsy: Time is brain? Neurology 89 (5). https://doi.org/10.1212/WNL.0000000000004176. 506–16. (PubMed PMID: 28687722; PubMed Central PMCID: PMCPMC5539734).

Campos, B.M., Coan, A.C., Beltramini, G.C., Liu, M., Yassuda, C.L., Ghizoni, E., et al., 2015. White matter abnormalities associate with type and localization of focal epileptogenic lesions. Epilepsia 56 (1), 125–132. https://doi.org/10.1111/epi.12871. (PubMed PMID: 25545559).

Cendes, F., Sakamoto, A.C., Spreafico, R., Bingaman, W., Becker, A.J., 2014. Epilepsies associated with hippocampal sclerosis. Acta Neuropathol. 128 (1), 21–37. https://doi.org/10.1007/s00401-014-1292-0. (PubMed PMID: 24823761).

Chassoux, F., Rodrigo, S., Semah, F., Beuvon, F., Landre, E., Devaux, B., et al., 2010. FDG-PET improves surgical outcome in negative MRI Taylor-type focal cortical dysplasias. Neurology 75 (24), 2168–2175. https://doi.org/10.1212/WNL.0b013e31820203a9. (PubMed PMID: 21172840).

Chiang, S., Levin, H.S., Wilde, E., Haneef, Z., 2016. White matter structural connectivity changes correlate with epilepsy duration in temporal lobe epilepsy. Epilepsy Res. 120, 37–46. https://doi.org/10.1016/j.eplepsyres.2015.12.002. (PubMed PMID: 26709881; PubMed Central PMCID: PMCPMC4740226).

Coan, A.C., Kubota, B., Bergo, F.P., Campos, B.M., Cendes, F., 2014. 3T MRI quantification of hippocampal volume and signal in mesial temporal lobe epilepsy improves detection of hippocampal sclerosis. AJNR Am. J. Neuroradiol. 35 (1), 77–83. https://doi.org/10.3174/ajnr.A3640. PubMed PMID: 23868151.

Concha, L., Beaulieu, C., Collins, D.L., Gross, D.W., 2009. White-matter diffusion abnormalities in temporal-lobe epilepsy with and without mesial temporal sclerosis. J. Neurol. Neurosurg. Psychiatry 80 (3), 312–319. Epub 2008/11/04. https://doi.org/10.1136/jnnp.2007.139287 (PubMed PMID: 18977826).

Deleo, F., Thom, M., Concha, L., Bernasconi, A., Bernhardt, B.C., Bernasconi, N., 2018. Histological and MRI markers of white matter damage in focal epilepsy. Epilepsy Res. 140, 29–38. Epub 2017/12/12. https://doi.org/10.1016/j.eplepsyres.2017.11.010 (PubMed PMID: 29227798).

Engel Jr., J., 1996. Introduction to temporal lobe epilepsy. Epilepsy Res. 26 (1), 141–150 (PubMed PMID: 8985696).

Fujiyoshi, K., Hikishima, K., Nakahara, J., Tsuji, O., Hata, J., Konomi, T., et al., 2016. Application of q-space diffusion MRI for the visualization of white matter. J. Neurosci. 36 (9), 2796–2808. https://doi.org/10.1523/JNEUROSCI.1770-15.2016. (PubMed PMID: 26937016).

Kamagata, K., Hatano, T., Okuzumi, A., Motoi, Y., Abe, O., Shimoji, K., et al., 2016. Neurite orientation dispersion and density imaging in the substantia nigra in idiopathic Parkinson disease. Eur. Radiol. 26 (8), 2567–2577. https://doi.org/10.1007/s00330-015-4066-8. (PubMed PMID: 26515546).

Kashyap, R., Dondi, M., Paez, D., Mariani, G., 2013. Hybrid imaging worldwide-challenges and opportunities for the developing world: a report of a technical meeting organized by IAEA. Semin. Nucl. Med. 43 (3), 208–223. https://doi.org/10.1053/j.semnuclmed.2013.02.001. (PubMed PMID: 23561459).

Keller, S.S., Schoene-Bake, J.C., Gerdes, J.S., Weber, B., Deppe, M., 2012. Concomitant fractional anisotropy and volumetric abnormalities in temporal lobe epilepsy: cross-sectional evidence for progressive neurologic injury. PLoS One 7 (10), e46791. https://doi.org/10.1371/journal.pone.0046791. (PubMed PMID: 23071638; PubMed Central PMCID: PMCPMC3469561).

Kuba, R., Tyrlikova, I., Chrastina, J., Slana, B., Pazourkova, M., Hemza, J., et al., 2011. "MRI-negative PET-positive" temporal lobe epilepsy: invasive EEG findings, histopathology, and postoperative outcomes. Epilepsy Behav. 22 (3), 537–541. https://doi.org/10.1016/j.yebeh.2011.08.019. (PubMed PMID: 21962756).

Kumar, A., Chugani, H.T., 2013. The role of radionuclide imaging in epilepsy, part 1: sporadic temporal and extratemporal lobe epilepsy. J. Nucl. Med. 54 (10), 1775–1781. https://doi.org/10.2967/jnumed.112.114397. (PubMed PMID: 23970368).

Lemkaddem, A., Daducci, A., Kunz, N., Lazeyras, F., Seeck, M., Thiran, J.P., et al., 2014. Connectivity and tissue microstructural alterations in right and left temporal lobe epilepsy revealed by diffusion spectrum imaging. Neuroimage Clin. 5https://doi.org/10.1016/j.nicl.2014.07.013. 349–58. (PubMed PMID: 26236626; PubMed Central PMCID: PMCPMC4519999).

Leonardi, M., Ustun, T.B., 2002. The global burden of epilepsy. Epilepsia 43 (Suppl. 6), 21–25 (Epub 2002/08/23. PubMed PMID: 12190974).

Loi, R.Q., Leyden, K.M., Balachandra, A., Uttarwar, V., Hagler Jr., D.J., Paul, B.M., et al., 2016. Restriction spectrum imaging reveals decreased neurite density in patients with temporal lobe epilepsy. Epilepsia 57 (11). https://doi.org/10.1111/epi.13570. 1897–906. (PubMed PMID: 27735051; PubMed Central PMCID: PMCPMC5118147).

Lopinto-Khoury, C., Sperling, M.R., Skidmore, C., Nei, M., Evans, J., Sharan, A., et al., 2012. Surgical outcome in PET-positive, MRI-negative patients with temporal lobe epilepsy. Epilepsia 53 (2), 342–348. https://doi.org/10.1111/j.1528-1167.2011.03359.x. (PubMed PMID: 22192050).

Loscher, W., Schmidt, D., 2011. Modern antiepileptic drug development has failed to deliver: ways out of the current dilemma. Epilepsia 52 (4), 657–678. https://doi.org/10.1111/j.1528-1167.2011.03024.x. (PubMed PMID: 21426333).

Mueller, S.G., Laxer, K.D., Cashdollar, N., Buckley, S., Paul, C., Weiner, M.W., 2006. Voxel-based optimized morphometry (VBM) of gray and white matter in temporal lobe epilepsy (TLE) with and without mesial temporal sclerosis. Epilepsia 47 (5). https://doi.org/10.1111/j.1528-1167.2006.00512.x. 900–7. (PubMed PMID: 16686655; PubMed Central PMCID: PMCPMC2744650).

Ota, M., Noda, T., Sato, N., Hidese, S., Teraishi, T., Setoyama, S., et al., 2018. The use of diffusional kurtosis imaging and neurite orientation dispersion and density imaging of the brain in major depressive disorder. J. Psychiatr. Res. 98, 22–29. https://doi.org/10.1016/j.jpsychires.2017.12.011. (PubMed PMID: 29272758).

Otte, W.M., van Eijsden, P., Sander, J.W., Duncan, J.S., Dijkhuizen, R.M., Braun, K.P., 2012. A meta-analysis of white matter changes in temporal lobe epilepsy as studied with diffusion tensor imaging. Epilepsia 53 (4), 659–667. https://doi.org/10.1111/j.1528-1167.2012.03426.x. (PubMed PMID: 22379949).

Rathore, C., Radhakrishnan, K., 2015. Concept of epilepsy surgery and presurgical evaluation. Epileptic. Disord. 17 (1), 19–31. quiz. https://doi.org/10.1684/epd.2014.0720 (PubMed PMID: 25652945).

Reyes, A., Uttarwar, V.S., Chang, Y.A., Balachandra, A.R., Pung, C.J., Hagler Jr., D.J., et al., 2018. Decreased neurite density within frontostriatal networks is associated with executive dysfunction in temporal lobe epilepsy. Epilepsy Behav. 78, 187–193. https://doi.org/10.1016/j.yebeh.2017.09.012. (PubMed PMID: 29126704; PubMed Central PMCID: PMCPMC5756677).

Rostampour, M., Hashemi, H., Najibi, S.M., Oghabian, M.A., 2018. Detection of structural abnormalities of cortical and subcortical gray matter in patients with MRI-negative refractory epilepsy using neurite orientation dispersion and density imaging. Phys. Med. 48, 47–54. https://doi.org/10.1016/j.ejmp.2018.03.005. (PubMed PMID: 29728228).

Smith, S.M., Jenkinson, M., Johansen-Berg, H., Rueckert, D., Nichols, T.E., Mackay, C.E., et al., 2006. Tract-based spatial statistics: voxelwise analysis of multi-subject diffusion data. NeuroImage 31 (4), 1487–1505. https://doi.org/10.1016/j.neuroimage.2006.02.024. (PubMed PMID: 16624579).

Sone D, Matsuda H, Ota M, Maikusa N, Kimura Y, Sumida K, et al. Graph Theoretical analysis of structural neuroimaging in temporal lobe epilepsy with and without psychosis. PLoS One. 2016a;11(7):e0158728. doi: https://doi.org/10.1371/journal.pone.0158728. (PubMed PMID: 27385130; PubMed Central PMCID: PMCPMC4934878).

Sone, D., Ota, M., Maikusa, N., Kimura, Y., Sumida, K., Yokoyama, K., et al., 2016b. White matter abnormalities in patients with temporal lobe epilepsy and amygdala enlargement: Comparison with hippocampal sclerosis and healthy subjects. Epilepsy Res. 127, 221–228. https://doi.org/10.1016/j.eplepsyres.2016.09.011. (PubMed PMID: 27635630).

Sone, D., Watanabe, M., Ota, M., Imabayashi, E., Rokicki, J., Maikusa, N., et al., 2018. Subtle abnormality in neurite dispersion in idiopathic generalized epilepsy detected by an advanced diffusion imaging technique. Epilepsy Seizure 10 (1), 33–43. https://doi.org/10.3805/eands.10.33.

Thom, M., 2014. Review: hippocampal sclerosis in epilepsy: a neuropathology review. Neuropathol. Appl. Neurobiol. 40 (5), 520–543. https://doi.org/10.1111/nan.12150. (PubMed PMID: 24762203; PubMed Central PMCID: PMC4265206).

Wakana, S., Caprihan, A., Panzenboeck, M.M., Fallon, J.H., Perry, M., Gollub, R.L., et al., 2007. Reproducibility of quantitative tractography methods applied to cerebral white matter. NeuroImage 36 (3). https://doi.org/10.1016/j.neuroimage.2007.02.049. 630–44. (PubMed PMID: 17481925; PubMed Central PMCID: PMCPMC2350213).

Whelan, C.D., Altmann, A., Botia, J.A., Jahanshad, N., Hibar, D.P., Absil, J., et al., 2018. Structural brain abnormalities in the common epilepsies assessed in a worldwide ENIGMA study. Brain 141 (2), 391–408. https://doi.org/10.1093/brain/awx341. (PubMed PMID: 29365066; PubMed Central PMCID: PMCPMC5837616).

Wiebe, S., Blume, W.T., Girvin, J.P., Eliasziw, M., 2001. A randomized, controlled trial of surgery for temporal-lobe epilepsy. N. Engl. J. Med. 345 (5), 311–318. Epub 2001/08/04. https://doi.org/10.1056/nejm200108023450501 (PubMed PMID: 11484687).

Winston, G.P., 2015. The potential role of novel diffusion imaging techniques in the understanding and treatment of epilepsy. Quant Imaging Med Surg. 5 (2), 279–287. https://doi.org/10.3978/j.issn.2223-4292.2015.02.03. (PubMed PMID: 25853085; PubMed Central PMCID: PMCPMC4379320).

Winston, G.P., Micallef, C., Symms, M.R., Alexander, D.C., Duncan, J.S., Zhang, H., 2014. Advanced diffusion imaging sequences could aid assessing patients with focal cortical dysplasia and epilepsy. Epilepsy Res. 108 (2). https://doi.org/10.1016/j.eplepsyres.2013.11.004. 336–9. (PubMed PMID: 24315018; PubMed Central PMCID: PMCPMC3969285).

Zhang, H., Schneider, T., Wheeler-Kingshott, C.A., Alexander, D.C., 2012. NODDI: practical in vivo neurite orientation dispersion and density imaging of the human brain. NeuroImage 61 (4), 1000–1016. https://doi.org/10.1016/j.neuroimage.2012.03.072. (PubMed PMID: 22484410).